FULL PAPER

Temperature-Sensitive Nanocapsules for Controlled Drug Release Caused by Magnetically Triggered Structural Disruption

By *Ting-Yu Liu, Kun-Ho Liu, Dean-Mo Liu, San-Yuan Chen,* and *I-Wei Chen**

Self-assembled nanocapsules containing a hydrophilic core and a crosslinked yet thermosensitive shell are successfully prepared using poly(ethylene-oxide)-poly(propylene-oxide)-poly(ethylene-oxide) block copolymers, 4-nitrophenyl chloroformate, gelatin, and 1-ethyl-3-(3-dimethylaminopropyl) carbodiimide. The core is further rendered magnetic by incorporating iron oxide nanoparticles via internal precipitation to enable externally controlled actuation under magnetic induction. The spherical nanocapsules exhibit a hydrophilic-to-hydrophobic transition at a characteristic but tunable temperature reaching 40 °C, triggering a size contraction and shrinkage of the core. The core content experiences very little leakage at 25 °C, has a half life about 5 h at 45 °C, but bursts out within a few minutes under magnetic heating due to iron oxide coarsening and core/shell disruption. Such burst-like response may be utilized for controlled drug release as illustrated here using a model drug Vitamin B12.

1. Introduction

Thermally sensitive drug delivery carriers that can be remotely actuated are attractive for therapeutic and patient management. One possible approach is to use a composite carrier made of a magnetic core inside a thermally sensitive polymer micelle with a temperature-dependent drug release profile, so that when the core is self-heated in response to an external magnetic stimulus it triggers the release of the drug contained within the micelle. The idea is a natural extension of two concepts, i) magnetic heating that has been used for tumor treatment (i.e., hyperthermia) and ii) thermally induced volume/hydrophobicity transition that has been observed in certain polymers and hydrogels. However, composite magnetic nanoparticles that combine attributes of acceptable biocompatibility, fast actuation, high on/off ratio of drug release and an operation temperature at about the physiological temperature will require a careful design of material constituents and their self-assembly. Here we undertake such a study using poly (ethylene-oxide)-poly(propylene-oxide)-poly (ethylene-oxide) (PEO-PPO-PEO) copolymers and iron oxide nanoparticles as building blocks for the magnetic nanoparticle and vitamin B12 as a model drug; crosslinking agents were also introduced to modify the composite nanostructure.

As background, the idea of using external magnetic fields to achieve drug release from polymer composites was first reported by Kost et al. who demonstrated insulin release from a magnetic composite of ethylene vinyl acetate under a low frequency magnetic field.[1–2] Recently, De Paoli et al.[3] reported magnetically enhanced dextran release (which simulates protein release) from a magnetic nanocomposite made of a collagen gel. Magnetic biocompatible iron oxide nanoparticles were used in the latter study as in our previous work on ferrogels,[4] but they both involved bulk gels instead of colloids. Colloids of iron oxide nanoparticles can be used as a delivery vehicle: for example, a single-strand DNA can be grafted to the nanoparticle; a dye-labeled complement can then be reversibly associated to or dissociated from it depending on the temperature.[5] On thermally sensitive polymers, Choi et al.[6] reported pluronic/heparin nanocapsules that exhibited a reversible (1000×) volume transition when cycled between 25 and 37 °C. Their study built on the well-known properties of PEO-PPO-PEO triblock polymers (biocompatible and commercially known as pluronic) that manifest a range of critical micellization temperature (CMT) for volume/hydrophobicity transition, but it further enhanced the volume change by crosslinking the outer shell. To aim at an unprecedentedly fast drug release under a remote magnetic trigger, we have combined these considerations in our design which contains i) a collapsible magnetic core of iron oxide immersed in a water solution of vitamin B12, ii) a fast-breathing nanosized two-layer shell of thermally responsive PEO-PPO-PEO polymer, and iii) a crosslinked outer shell that stabilizes the nanoshell while maintaining the CMT, the volume change and the drug release. The preparation procedure following the self-assembly schemes of Figure 1a and b, the experimental evidence (from transmission electron microscopy, dynamic light scattering) in support of the Schemes, and the thermal responses and drug release characteristics of the nanoparticles are described below.

[*] I.-W. Chen T.-Y. Liu
Department of Materials Science and Engineering
University of Pennsylvania
Philadelphia, PA 19104-6272 (USA)
E-mail: iweichen@seas.upenn.edu
T.-Y. Liu, K.-H. Liu, D.-M. Liu, S.-Y. Chen
Department of Materials Science and Engineering
National Chiao Tung University
Hsinchu, Taiwan (R.O.C)

DOI: 10.1002/adfm.200801304

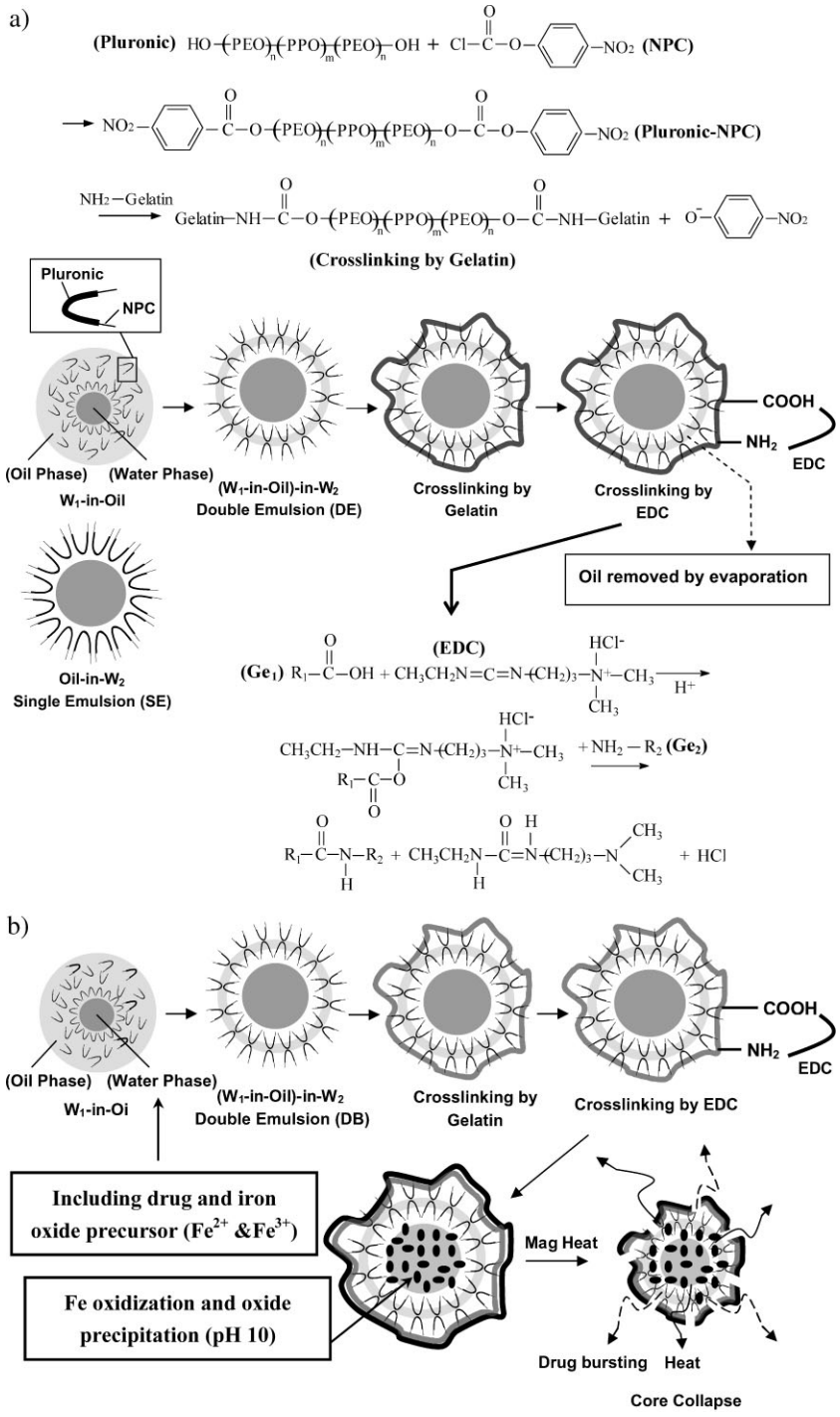

Figure 1. a) Chemical reactions, self-assembly and schematic structures of various nanocapsules, b) procedure for encapsulating drug and iron oxide into nanocapsules and events triggered by magnetic heating: volume shrinkage, core collapse, heat conduction, and drug release.

2. Results

2.1. Structure of NPC-Activated F127 and F68

^{1}H NMR spectra are shown in the Supporting Information Figure S1 for F127-NPC and F68-NPC in deuterated chloroform ($CDCl_3$) solution. The activated polymer differs from the unactivated one in that the terminal alcohols on PEO-PPO-PEO are converted into nitrophenyl groups in a chloraformate environment. This is supported by the spectra which give evidence of protons in the ortho (*o*)-position (near the $-NO_2$ side) in the nitrophenyl (NO_2Ph) group, protons in the meta (*m*)-position (near the –COO side) in the nitrophenyl group, and signals associated with $-NO_2Ph-OCOO-CH_2$ which identifies NPC's attachment to the –OH group of PEO. Other structures indicate a PEO-PPO-PEO backbone including the PEO–CH_2–units and the PPO–CH_3 units.

2.2. Size of Nanocapsules

Double-layer F127-NPC and F68-NPC nanocapsules of different sizes at 25 °C are shown in Figure 2. They are F127-NPC-DE in Figure 2a and F68-NPC-DE in Figure 2b, both in the form of double-emulsion (W_1-in-oil-in-W_2), to be compared with single-emulsion (oil-in-W_2) nanocapsules (F127-NPC-SE and F68-NPC-SE) and W_1-in-oil inverse micelles (F127-NPC-W1-in-oil and F68-NPC-W1-in-oil in the insets). For both polymers, the size of the nanocapsules decreases with increasing content of the polymer, but the size is always smaller for the F127-series than for the F68-series. Regardless of the polymer used, the resulting nanocapsules normally show a size decrease in the order of DE > SE > W_1-in-oil. Moreover, in the case of the DE and SE series, a constant size is reached when the polymer concentration is around 1.0 g mL^{-1}. This critical concentration for maintaining a constant size was employed in all subsequent experiments.

2.3. Size Variation of the Crosslinked Nanocapsules

The size distributions of double-layer nanocapsules F127-NPC-DE before and after gelatin-cross-linking are shown in Figure 3. With the addition of 1 mg mL^{-1} gelatin in the W_2 phosphate buffered solution (PBS) solution, the size increases slightly from a peak value of 28.4–35.6 nm. This increment is mostly caused by a small increase in the CMT (from 21.9 to 22.8 °C, see Table 1) due to the presence of gelatin; this point will be supported by other CMT data to be detailed later. A high concentration of gelatin, e.g., 5 and 10 mg ml^{-1}, broadens the size distribution considerably and causes a secondary peak at a very large size (Fig. 3, inset),

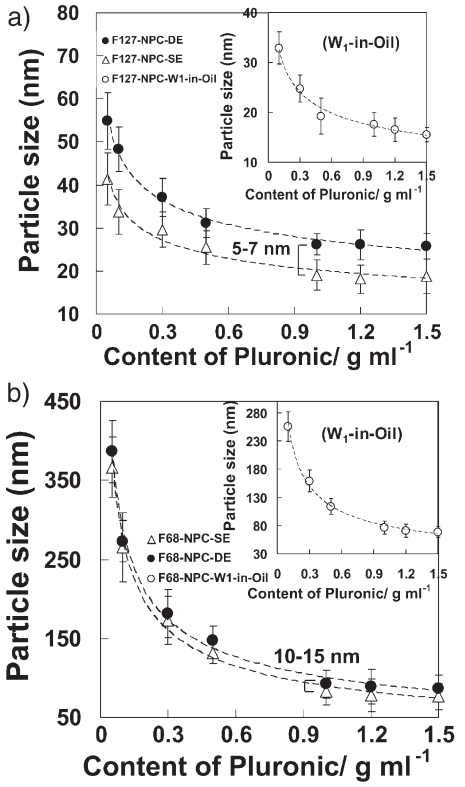

Figure 2. Diameter of nanocapsules measured by DLS of a) F127 and b) F68 series. DE is a water-in-oil-in-water structure, SE is an oil-in-water structure, and the inset is a water-in-oil structure.

indicating agglomeration has occurred possibly by forming cross-linking bridges between nanocapsules. Accordingly, an optimal concentration of 1 mg ml^{-1} gelatin was selected in the W_2 PBS solution for further study.

Likewise, the size of nanocapsules after the second cross-linking using EDC was measured where a size decrease from 35.6 to 30.5 nm was found as shown in Table 1 (d_{RT}). A similar trend was found for F68 nanocapsules (Table 1). Since the change in

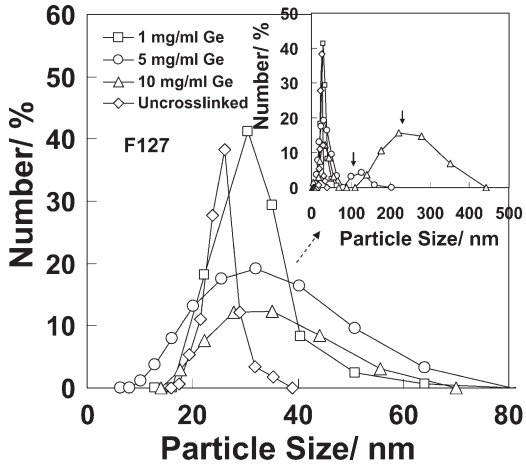

Figure 3. Diameter distribution of F127-NPC nanocapsules after cross-linking by different amount of gelatins. Inset: same with a more extended size range.

CMT due to EDC, from 22.8 to 22.4 °C (Table 1) is relatively small, the size shrinkage may be attributed to a more compact structure after $-NH_2$ and –COOH cross-linking.

A freshly formed F68-NPC-DE nanocapsule after double emulsion has a spherical geometry as shown in the TEM image in Figure 4a. After washing five times and dialysis, the nanocapsule (Fig. 4b) is about 100 nm, which is very close to the DLS peak value (see Table 1). After gelatin and EDC cross-linking there is little further change in size but a higher electron density has developed on the particle skin (Fig. 4c).

2.4. Precipitation and Encapsulation of Iron Oxide

Evidence for the formation of iron oxide (IO) nanocrystals inside the nanocapsules is shown in Figure 5 for F68-NPC-DE after gelatin and EDC crosslinking. The size is again about 100 nm (Fig. 5a) and the skin (6–8 nm) is clearly of a higher electron

Table 1. Characteristics of F127 and F68-series nanocapsules at 1 g mL^{-1} pluronic.

Samples	Non-activated		NPC-activated		Gel-modified		EDC-modified		Iron oxide
	F127	F68	F127-NPC	F68-NPC	F127-Ge	F68-Ge	F127-EDC	F68-EDC	F68-IO
CMT [°C]	25.8	43.2	21.9	39.3	22.8	40.1	22.4	39.6	40.5
Size and size ratio									
d_{max} [nm][a]	115.7	143.1	78.2	86.4	91.4	105.3	82.1	97.0	113.1
d_{RT} [nm][b]	60.8	135.2	28.4	85.3	35.6	101.5	30.5	94.2	108.3
d_{min} [nm][c]	23.6	22.1	27.3	22.0	27.3	23.8	25.1	23.6	43.1
d_{max}/d_{min}	4.9	6.5	2.9	3.9	3.3	4.4	3.2	4.1	2.6
Drug release (ratio)									
$Ratio_{45/4}$[d]	–	12.1	–	–	–	39.4	–	45.5	57.3
$Ratio_{45/25}$[e]	–	5.9	–	–	–	11.6	–	14.3	17.2
$Ratio_{45/37}$[f]	–	3.5	–	–	–	6.8	–	8.2	9.5

[a] 10 °C for F127-series and 20 °C for F68-series. [b] Room temperature (25 °C). [c] 40 °C for F127-series and 50 °C for F68-series. [d] Ratio of cumulative percentage release after 6 h at 45 °C, to that at 4 °C. [e] Ratio of cumulative percentage release after 6 h at 45 °C, to that at 25 °C. [f] Ratio of cumulative percentage release after 6 h at 45 °C, to that at 37 °C.

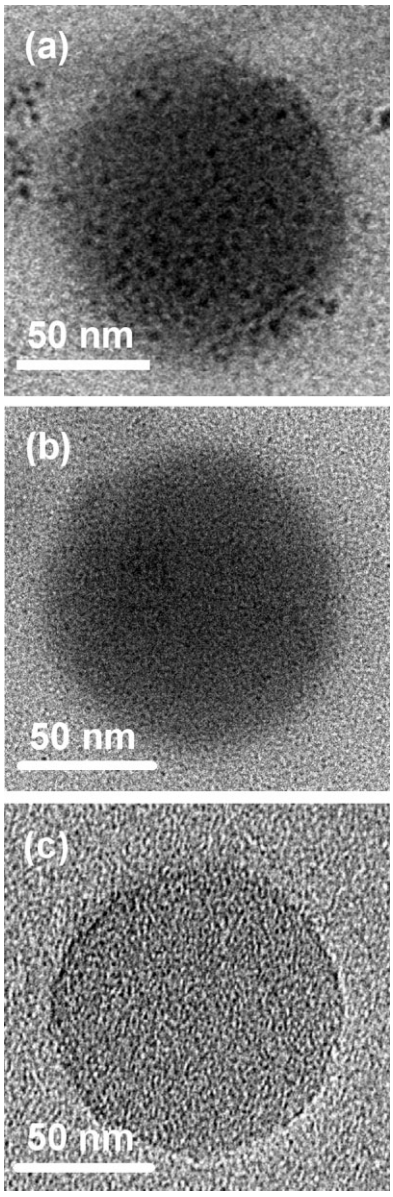

Figure 4. Transmission electron micrographs of F68 series nanocapsules a) before dialysis, b) after repeated washing and dialysis, and c) after gelatin and EDC cross-linking.

density (Fig. 5b). In addition, there is evidence of chain crystallization (periodic fringes in highlighted boxes in Fig. 5b) in the corona of the nanocapsules. At higher magnification, the nanocapsule shows a contrast modulation due to particles of a size of 5–10 nm (Fig. 5c). These particles are crystalline as evidenced by the selected area diffraction pattern in Figure 5d, indicating the Fe_3O_4 crystal planes of [200], [311], [400], and [511].

2.5. Thermosensitive Behavior and CMT

Nanocapsules exhibit thermally sensitive behavior similar to that of the PEO-PPO-PEO polymer showing shrinkage above the CMT, signifying a hydrophilic/hydrophobic transition. The CMT

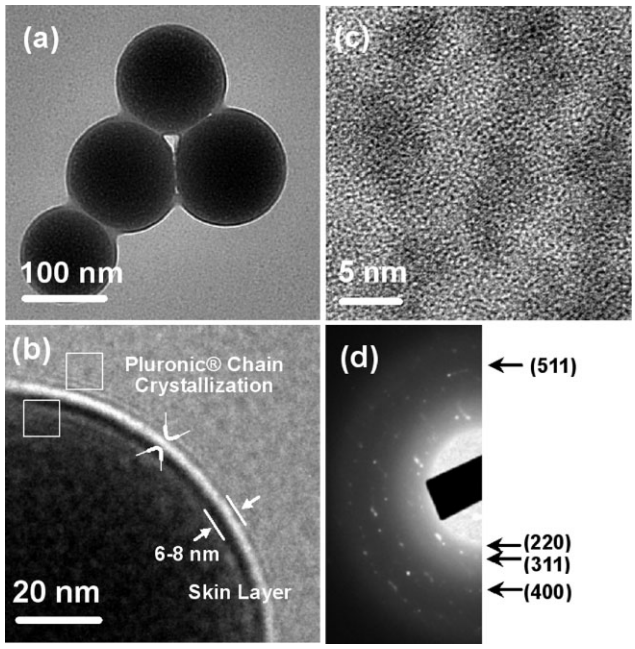

Figure 5. Transmission electron micrographs of a) fully cross-linked F68 nanocapsules containing iron oxide nanoparticles, b) a high electron density shell of a thickness about 6–8 nm, with a corona region highlighted to show periodic modulation presumably due to polymer chain crystallization, and c) contrast modulation due to iron oxide nanoparticles. d) Selected area electron (SAE) diffraction pattern of several single crystals of various orientations.

and volume change can be altered by the chemical modification (e.g., NPC and gelatin) which provides a way for fine tuning to suit the drug release application. This was determined by measuring the capsule size as a function of temperature, shown in Figure 6, where a transition is manifested by a large volume shrinkage. For data quantification, the CMT is defined as the inflection point of the curve, and a size ratio is defined using d_{max}/d_{min} where d_{max} is the maximum particle diameter below the CMT at the lowest

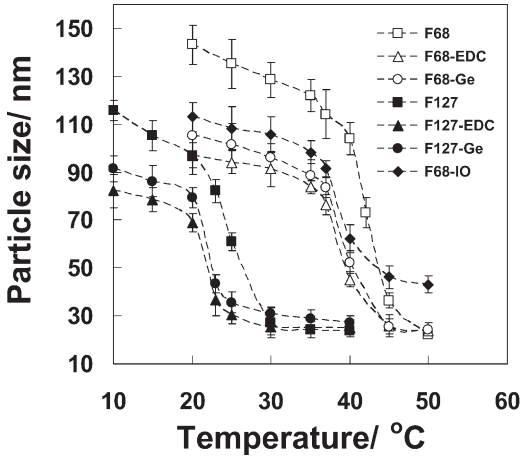

Figure 6. Diameter of nanocapsules measured by DLS decreases abruptly at about CMT. F68 series has higher CMT than F127 series.

measurement temperature and d_{min} is the minimum particle diameter above the CMT at the highest measurement temperature. It is then clear that the larger size of the F68 series is mainly due to a much higher CMT (43.2 °C) than that of F127 (25.8 °C). (This largely reflects a higher EO/PO ratio in F68, which is 5.24, compared to that of F127, which is 3.08.) In addition, there is a slight decrease (about 4 °C) of CMT for activated polymers, presumably because NPC addition causes an increase of hydrophobicity. In contrast, the increase (about 1 °C) in CMT is small in gelatin-cross-linked nanocapsules, and the increase (about 0.5 °C) when EDC was added is even smaller. These changes of CMT summarized in Table 1 are consistent with the size data at 25 °C.

The size ratio of the nanocapsule significantly decreases when it is cross-linked by gelatin, but the further decrease is small when it is additionally cross-linked by EDC (row 5 in Table 1). Incorporating IO into F68-EDC decreases the size ratio from 4.1 (corresponding to a volume ratio of about 67) to 2.6 (corresponding to a volume ratio of 18); see row 6 in Table 1. From Figure 6, it is clear that the IO addition causes a decrease of d_{max} and an increase of d_{min}, so both the hydrophilic ''swollen'' state and the hydrophobic ''shrunk'' state appear to be sterically constrained from reaching their respective fully relaxed sizes. Since the F68 series shows a higher ratio than the F127 series, it was selected to encapsulate B12 for drug release studies.

2.6. Drug Release with and without Magnetic Heating

Cumulative release of vitamin B12 as a function of time is shown in Figure 7 for four F68 series double-layer nanocapsules: F68 (neat polymer), F68-Ge (gelatin cross-linked), F68-EDC (further EDC crosslinked), and F68-IO (IO-containing and fully cross-linked). The data were obtained at four temperatures, 4, 25, 37, and 45 °C, and fitted with Equation (2) (see Experimental Section) giving the fitting parameters listed in Table 2. Although some data (those with n far away from 0.5) do not warrant an interpretation based on diffusion mechanisms, to allow a more quantitative comparison we nevertheless force-fit the data with the following expression[7] to obtain the apparent ''diffusivity'' D_e listed in Table 2,

$$\frac{M_t}{M_\infty} = 4\left(\frac{D_e t}{\pi d^2}\right)^{1/2} \quad (1)$$

This fitting was performed for $M_t/M_\infty < 0.6$. It is then clear that there is a systematic reduction of D_e in the order of F68 > F68-Ge > F68-EDC ~ F68-EDC-IO, in addition to the obvious increase of D_e with the temperature. This indicates that vitamin B12 release is a thermally activated process, and crosslinking of the shell slows down the release.

From a practical viewpoint, a large on/off ratio is desired. This would require a very large ratio of the 45 °C release to that at either the physiological temperature (37 °C) or the storage/application temperature (4 °C/25 °C). These ratios are listed in Table 1 using the cumulative release after 6 h. It is clear that crosslinking significantly increases the ratio, and the incorporation of IO does not cause any adverse effect. The ratio comparing 45 °C (>CMT) and 37 °C (<CMT) is 9.5 indicating a clear effect of the transition. Meanwhile, the slow release at 4 and 25 °C being only 1/57 and 1/17, respectively of that at 45 °C assures a long shelf time of this drug carrier.

Lastly, the effect of magnetic heating (with the solution held in a water bath of 15 °C) is shown in Figure 7 (see symbol ✳) which evidently has a much larger cumulative release in just a few minutes: about 40% cumulative release is reached in the first 5 min, which is about 20 times the rate normally achieved at 45 °C. According to Figure 6 the shrinkage is already nearly complete at 45 °C, so magnetic heating should not cause much

Table 2. Summary of fitting constants (n and k) for cumulative release, apparent diffusivity, and estimated half life t_{50} reaching 50% cumulative release.

Sample	Temp. [°C]	n	$k \times 10^3$	$D_e \times 10^9$ [μm^2 min^{-1}]	t_{50} [h]
F68	4	0.781	0.62	0.96	41.3
	25	0.77	1.22	3.63	27.5
	37	0.762	2.00	8.49	16.3
	45	0.588	28.15	177.12	2.1
F68-Ge	4	0.799	0.10	0.03	270.6
	25	0.783	0.47	0.62	82.9
	37	0.773	0.79	1.73	42.1
	45	0.603	18.26	87.57	3.9
F68-EDC	4	0.808	0.07	0.02	277.8
	25	0.787	0.33	0.31	83.1
	37	0.776	0.59	0.91	41.5
	45	0.616	14.18	60.67	6.0
F68-EDC-IO	4	0.846	0.05	0.02	416.7
	25	0.84	0.24	0.25	92.3
	37	0.833	0.41	0.85	41.6
	45	0.615	15.71	73.02	4.8

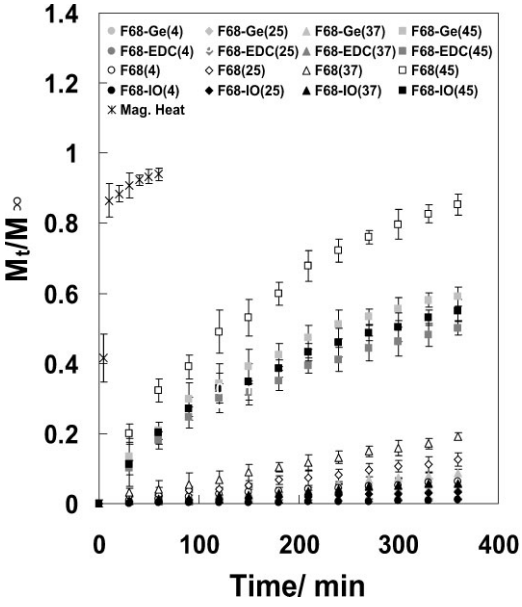

Figure 7. Cumulative vitamin B12 release as a function of time for four F68 series nanocapsules at various temperatures from 4 to 45 °C as indicated in the parentheses. Many low temperature data are too close to be resolved on this graph but their relative order is the same as 45 °C. Release data under an external magnetic field for F68-IO also shown (mag heat).

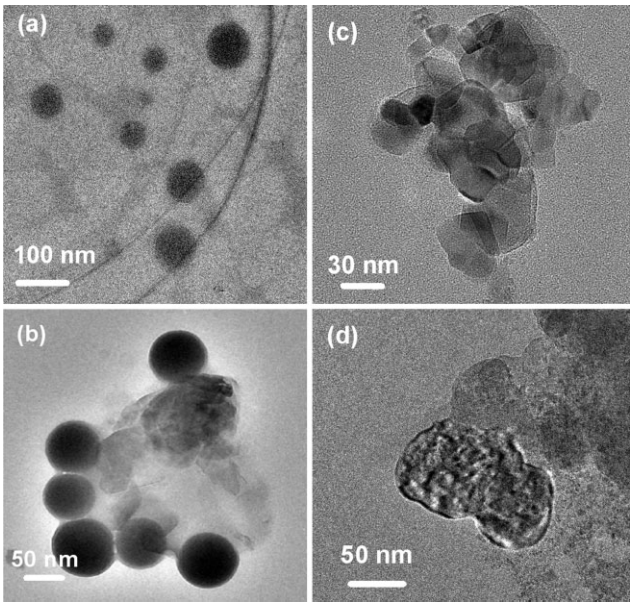

Figure 8. Transmission electron micrographs of F68-IO nanocapsules showing a) uneven shrinkage after heating to 45 °C; b) unevenly restructured core and shell after magnetic heating, with c) structure disruption and faceting, and d) crystal coarsening.

more squeezing of the core. Therefore, the burst-like accelerated release under magnetic heating cannot be attributed to the volume change alone.

The TEM micrograph presented in Figure 8a shows that when nanocapsules experienced a thermal excursion to 45 °C but without a magnetic field they remained spherical although some (smaller spheres in Fig. 8a) had apparently shrunk indicating drug release may have occurred. In contrast, after exposure to a magnetic field many nanocapsules lost their spherical shape, as shown in Figure 8b–d. Some appeared to be faceted suggesting recrystalization (Fig. 8c); others have coarsened considerably suggesting grain growth (Fig. 8d). Clearly, these changes are highly disruptive which may correspond to the scenario depicted in Figure 1b leading to a burst of drug release.

3. Discussion

3.1. Shell Thickness of Nanocapsules

Although double-layer microcapsules typically have a water-in-oil-in-water configuration, following Choi et al.[6] we have removed the oil layer by evaporation, so that the hydrophobic sides of the two layers are presumably in contact. According to Figure 2, the difference between the size of the double-emulsion nanocapsule and the single-emulsion nanocapsule (oil-in-W_2) is a constant, about 5–7 nm in the F127 series and 10–15 nm in the F68 series. This thickness difference may represent the thickness of a single-layer. In an earlier report, a small-angle neutron scattering measurement of pluronic 105 (containing $(EO)_{37}(PO)_{56}(EO_{37})$ blocks) gave a double-layer width of 9.5 nm, which is of the same order of magnitude.[8]

For comparison, we next estimate the single-layer thickness using another method. From Figure 2, we see that there is a critical concentration of 1 g pluronic/1 mL oil above which a constant size is reached for both types (F127 and F68) of nanocapsules. This suggests that the excess pluronic is dissolved and not incorporated in the shell. Since the density of pluronic and oil is similar, the above critical concentration corresponds to a volume ratio $V_{\text{pluronic}}/V_{\text{oil}}$ about 1 for the ''equilibrated'' oil-in-water micelles of single-shell. The single-shell thickness of such equilibrated micelle can be estimated from the size data in Figure 2 and the spherical geometry with a core radius r and a shell thickness a: the shell to (oil) core volume ratio is about $r/3a$ and the diameter $2r+2a$ should correspond to the steady-state size in Figure 2 (the single-emulsion nanocapsules). From this, the single-shell thickness is estimated to be about 2.4 nm for F127 and 10.3 nm for F68, at 25 °C. These values fall in the same range as estimated before.

3.2. Stability of Nanocapsules and Controlled Drug Release

Nanocapsules reported in this work are highly stable at room temperature and below. This is reflected in the low release rate at 4 and 25 °C. An estimate of the half life (t_{50}) required to reach 50% release may be obtained by replotting Figure 7 in a log–log form to extrapolate it to $M_t/M_\infty = 0.5$ (figure not shown).[9] These half lives are listed in Table 2, and they range from 40 to 400 h indicating good (4 °C) storage stability. It is also clear that crosslinking the double-layer improves the stability, as reflected in both the half life and the apparent diffusivity D_e in Table 2.

According to Table 2, the exponent n decreases with increasing temperature gradually approaching 0.5, corresponding to diffusion-controlled release (Fickian diffusion). Taking the data at 45 °C and assuming a diffusion mechanism, then the diffusion distance (L) may be estimated by $L = (2D_e t)^{1/2}$ with t being the diffusion time. All the data in Figure 7 suggest that 50% release is reached at 45 °C after about 300 min. Meanwhile, the apparent diffusivity is of the order of 10^{-7} μm^2 min^{-1} according to Table 2. This leads to an estimate of L of 7.7 nm, which seems to correspond to the single-layer thickness of F68, or the half thickness of the double-layer micelles used in these experiments. At lower temperature, the exponent n rises toward one. This indicates that the diffusion of B12 across the PEO-PPO-PEO shell is either non-Fickian or there is some binding between them at the interface or inside the shell. Such behavior holds for all the F68-series nanocapsules no matter whether they are cross-linked/IO-containing or not. This is not surprising since they all share a very similar CMT (varying from 39.3 to 40.5 °C if we exclude unmodified F68, which has a CMT of 43.2 °C). This relatively high CMT is partially responsible for the excellent stability of the nanocapsules at room temperature and below.

3.3. Magnetic Heating and Core Restructure

Under magnetic heating, burst-like release was seen, which is likely due to the irreversible and disruptive changes shown in Figure 8. Such changes were clearly caused by a local temperature

increase inside the IO, which must reach several hundred degrees of centigrade since rapid diffusion in IO is not expected below 300 °C. This large temperature increase should not extend much beyond the IO/water interface since according to the standard heat conduction theory, the radial heat flux from a hot sphere is inversely proportional to the radius and the temperature rise is nearly completely dissipated within one radius from the sphere. This means that the temperature rise can be sustained only within 2–4 nm from the IO/water interface, given the initial size of IO of 5–7 nm according to Figure 5c).

In our experiment, cooling water was supplied to maintain a constant temperature in the water bath during magnetic heating. Using similar experimental configurations but without active cooling, an initial temperature rise of the water solution at a linear rate (R_W) of 0.1–1 °C s^{-1} has been reported.[10] Since the energy input to heat up the water comes entirely from the heat generated in the magnetic particles, we can calculate the heating rate R_{IO} of the IO nanoparticles in terms of R_W using $V_{IO}R_{IO}C_{IO} = (1 - V_{IO})R_WC_W$. Here V_{IO} is the volume fraction of IO relative to the solution, and C_W and C_{IO} are volumetric specific heat of water and IO, respectively. Our experiment and most experiments in the literature used $V_{IO} \sim 0.001$. Meanwhile, referring to the specific heat of Fe, O, and water, we estimate $C_W/C_{IO} \sim 1$. Therefore, the calculated R_{IO} is from 100 to 1000 °C s^{-1}, i.e., it takes at most a few seconds for the temperature to rise to several hundred degrees in IO before a steady state is reached. The steady-state temperature can be easily shown to scale as $G/\alpha r^2$ by balancing the heat conduction (with a thermal conductivity α) away from IO and the heat generation rate (G, per unit volume) within IO, which has a radius r. Without knowing the details of interface heat transfer at the nanoscale, though, a more definitive determination of the steady-state temperature is not yet possible.

Recently, TEM evidence was also reported for magnetically induced structural changes in nanosized IO that forms a shell around a SiO_2 core.[4] This observation is supportive of our results indicating a thermal effect on IO restructuring. Other studies have suggested possible changes, such as reversible pore size enlargement, in the polymer shell due to a magnetic force alone.[11] This is because the frequency used (300 Hz) in the above study was low enough to exert a distortion force but not high enough to generate any significant heat. Given the high frequency of our experiment and the rather slow Brownian relaxation of the shell (70 nm in size),[12] we believe the magnetic force was too fast to be followed by the IO and the nanocapsule to cause any shell distortion. Even if the force did cause a reversible distortion and pore enlargement, these relatively small and subtle changes are probably insignificant compared to the massive crystal coarsening and disruption evident in Figure 8.

4. Conclusions

(i) Self-assembled aqueous nanocapsules containing a hydrophilic core and a crosslinked yet temperature-sensitive shell have been successfully prepared using PEO-PPO-PEO triblock copolymers, 4-nitrophenyl chloroformate (NPC), gelatin, and 1-ethyl-3-(3-dimethylaminopropyl) carbodiimide. The core may be rendered magnetic by incorporating iron oxide (IO) nanoparticles that form via internal precipitation.

(ii) The nanocapsules are spherical exhibiting a hydrophilic-to-hydrophobic transition at a characteristic but tunable temperature (CMT) triggering a size contraction as much as 6.5 times. With crosslinking and IO filling the size contraction decreases to a ratio of 2.6, allowing a large contraction of the core volume exceeding 17 times.

(iii) The crosslinked nanocapsules with a CMT from 39 to 43 °C exhibit very little leakage at 4 °C and 25 °C with an estimated half life of 270–410 and 80–90 h, respectively, with or without IO. Their half life at 37 °C still exceeds 40 and 41.6 h, which decreases to about 5 h at 45 °C reflecting a diffusivity transition across the CMT.

(iv) Responding to external magnetic induction, magnetic nanocapsules undergo irreversible structure changes including IO crystal coarsening, core/shell disruption, and rapid release of 80% of the core content within 5 min. Such burst-like response may be utilized for controlled drug release as illustrated here using a model drug vitamin B12.

5. Experimental

Synthesis of Activated PEO-PPO-PEO Polymers (F127 and F68): We used two commercial PEO-PPO-PEO thermal-sensitive polymers, pluronic F127 and F68, (Sigma, USA) to form two series of core/shell nanocapsules in this study. F127 has a $(EO)_{100}(PO)_{65}(EO)_{100}$ block structure with an EO/PO ratio of 3.08, and F68 has a $(EO)_{76}(PO)_{29}(EO)_{76}$ block structure with an EO/PO ratio of 5.24. The polymer (20 g of F127 or F68) was first dissolved in 60 mL of methylene chloride (Fisher Scientific, USA). In a dropwise manner this solution was added to a stirred solution of methylene chloride (60 mL) containing NPC (2 g). The activation reaction of forming covalent bonds between NPC and pluronics proceeded with gentle stirring (5 h) at room temperature under a nitrogen atmosphere. The activated polymer (F127-NPC or F68-NPC) was precipitated, washed five times in ice-cold diethyl ether, and dried under vacuum. To determine the activation density, a known amount of F127-NPC or F68-NPC was treated with NaOH (0.2 N) at 25 °C (2 h). The concentration of NPC released in the aqueous phase was quantified spectrophotometrically at 410 nm.

Fabrication of Activated PEO-PPO-PEO Nanocapsules: Single-layer nanocapsules containing one layer of activated PEO-PPO-PEO were synthesized using a single-emulsification (SE)/solvent-evaporation method. An oil phase (methylene chloride solution, 1 mL) containing various amount of F127-NPC or F68-NPC (0.05–1.5 g) was added dropwise to a water phase (10 mL) (W_2, PBS) at pH 7.4. The mixture was sonicated (10 min) using an ultrasonic homogenizer (Virsonic, VirTis, USA) operating at 20 kHz to obtain oil-in-water micelles, F127-SE or F68-SE, as shown in Figure 1a.

Double-layer nanocapsules containing two layers of PEO-PPO-PEO were synthesized using a double-emulsification (DE)/solvent-evaporation method. The first water phase W_1 (PBS, 0.1 mL) was added dropwise to an oil phase (methylene chloride solution, 1 mL) containing various amount of F127-NPC or F68-NPC (0.05–1.5 g). The mixture was sonicated (10 min) to obtain water (W_1)-in-oil micelles. Next, the micelle solution was added dropwise to a second water phase W_2 (PBS, 10 mL). The mixture was again sonicated (10 min) to obtain W_1-in-oil-in-W_2 micelles. The sample was called F127-DE or F68-DE (or F127-NPC-DE and F68-NPC-DE to emphasize that the outer shell is NPC-activated.) These emulsion solutions were next dialyzed (dialysis membrane with an Mw cutoff of 14 000) and the product stored at 4 °C until further use. The oil phase (methylene chloride) can be removed by evaporation at 30 °C to leave a

double-layer micelle containing a W_1 core, yet itself suspended in the W_2 phase.

Fabrication of Double-Layer Cross-linked Nanocapsules: A schematic of the nanocapsules with a cross-linked shell is depicted in Figure 1a. Essentially, the F127-DE or F68-DE activated with NPC is cross-linked with gelatin (Sigma), a hydrolyzed natural protein polymer rich in amino and carboxyl groups. To introduce gelatin to these double-layer micelles, we modified the second step in their preparation and added gelatin of various amount (1–10 mg mL^{-1}) to the W_2 phase (PBS) prior to the addition of the W_1-in-oil micelles. The emulsion of the resultant W_1-in-oil-in-W_2 micelles was immediately transferred to a water bath at 4 °C and held for 24 h to crosslink gelatin. After that, the emulsion solution was stirred at 30 °C to remove residual methylene chloride until the solution became clear. In addition, the gelatin can be fully cross-linked with the (dropwise) addition of 1 mL of 0.1 M 1-ethyl-3-(3-dimethylaminopropyl) carbodiimide (EDC, Sigma) to the above solution, held at 4 °C (24 h) [13,14]. These emulsion solutions were also dialyzed and the product stored at 4 °C until further use. The product after the first-step cross-linking will be referred to as F127-Ge or F68-Ge, and the product after the second-step cross-linking will be referred to as F127-EDC or F68-EDC.

Encapsulation of Drug and Iron Oxide into Nanocapsules: The above procedure was modified to incorporate a model drug vitamin B12 (Sigma), a cobalamin, into the W_1 phase; then this phase was used to prepare the double-layer nanocapsules as before followed by cross-linking. The concentration used was 10 mg mL^{-1} vitamin B12 in 0.1 mL PBS. To incorporate iron oxide, we used in situ co-precipitation of Fe(II) and Fe(III) salts. Briefly, $FeCl_3 \cdot 6H_2O$ (Riedel-deHaën) (0.1 mL of 1.08 g mL^{-1}) and $FeCl_2 \cdot 4H_2O$ (Fluka) (0.4 g mL^{-1}), together with vitamin B12 (10 mg mL^{-1}) were mixed into PBS to form the W_1 phase; then this phase was used to prepare the double-layer nanocapsules as before. After the final cross-linking steps, the pH of the mixture solution was adjusted to 10 by adding ammonia solution (33%) under stirring, followed by heat treatment at 60 °C for 30 min to precipitate iron oxide particles, as shown in Figure 1b. This product will be referred to as F68-IO. Other washing and storage procedures are the same as before.

Drug Release Test: In vitro drug release from the W_1 core of various double-layer nanocapsules was evaluated by incubating the vitamin B12-containing nanocapsules in 20 mL of PBS at various temperatures. At specific time intervals, some PBS solution was withdrawn and its concentration of vitamin B12 was measured by UV spectrum (361 nm). The percentage cumulative release was determined from this concentration after normalizing it by the amount of the initially loaded vitamin B12. The data were analyzed in terms of various kinetic mechanisms by fitting it to the time law of the form [15,16].

$$\frac{M_t}{M_\infty} = kt^n \tag{2}$$

where M_t is the cumulative release after time t, M_∞ the cumulative release at time infinity, and k and n are fitting coefficients.

We attempted to increase the release rate by radio frequency magnetic heating generated by an induction heater (15 kW) operating at 50–100 kHz.[17,18] The configuration is similar to the one reported in the literature [5,10], with an induction (copper) coil of eight loops delivering a magnetic field (2.5 kA m^{-1}). The solution was kept at 15 °C through a water bath during the experiment. The amount of the PBS solution used was 10 mL containing 0.2 g nanocapsules. Other procedures were the same as described before.

Characterization of Size and Microstructure: The chemical structure of the activated polymers was characterized by proton nuclear magnetic resonance spectroscopy (^{1}H-NMR) to confirm the sites and degrees of substitution. The samples were dissolved in $CDCl_3$ and the spectra were recorded by an NMR spectrometer (Bruker Avance-500, operating at 500 MHz) equipped with a microprocessor-controlled gradient unit and an inverse-detection multinuclear BBI probe with an actively shielded z-gradient coil. For nanocapsule characterization, dynamic light scattering (DLS, zetasizer-3000HS, Malvern, UK) was used for size determination and microscopy was performed using a transmission electron microscope (TEM, JEM-2010, JEOL, Japan) operating at 200 kV.

Acknowledgements

This work was supported by the National Science Council of the Republic of China, Taiwan under contract nos. NSC96-2627-B-009-006 and NSC96-2113-M009-027-MY2, and by the US National Science Foundation under grant no. DMR- 05-20020 (MRSEC). Supporting Information is available online from Wiley InterScience or from the author.

Received: September 3, 2008
Revised: November 3, 2008
Published online: January 12, 2009

[1] J. Kost, R. Noecker, E. Kunica, R. Langer, *J. Biomed. Mater. Res.* **1985**, *19*, 935.
[2] J. Kost, J. Wolfrum, E. Kunica, R. Langer, *J. Biomed. Mater. Res.* **1987**, *21*, 1367.
[3] V. M. De Paoli, S. H. De Paoli Lacerda, L. Spinu, B. Ingber, Z. Rosenzweig, N. Rosenzweig, *Langmuir* **2006**, *22*, 5894.
[4] S. H. Hu, S. Y. Chen, D. M. Liu, C. S. Hsiao, *Adv. Mater.* **2008**, *20*, 2690.
[5] A. M. Derfus, G. V. Maltzahn, T. J. Harris, T. Duza, K. S. Vecchio, E. Ruoslahti, S. N. Bhatia, *Adv. Mater.* **2007**, *19*, 3932.
[6] S. H. Choi, J. H. Lee, S. M. Choi, T. G. Park, *Langmuir* **2006**, *22*, 1758.
[7] J. B. Leach, C. E. Schmidt, *Biomaterials* **2005**, *26*, 125.
[8] L. Guo, R. H. Colby, *J. Rheol.* **2001**, *45*, 1223.
[9] S. M. Ansell, S. A. Johnstone, P. G. Tardi, L. Lo, S. Xie, Y. Shu, T. O. Harasym, N. L. Harasym, L. Williams, D. Bermudes, B. D. Liboiron, W. Saad, R. K. Prud'homme, L. D. Mayer, *J. Med. Chem.* **2008**, *51*, 3288.
[10] D. H. Kim, D. E. Nikles, D. T. Johnson, C. S. Brazel, *J. Magn. Magn. Mater.* **2008**, *320*, 2390.
[11] Z. M. Lu, D. Prouty, Z. Guo, V. O. Golub, C. S. S. R. Kumar, Y. M. Lvov, *Langmuir* **2005**, *21*, 2042.
[12] R. E. Rosensweig, *J. Magn. Magn. Mater.* **2002**, *252*, 370.
[13] W. C. Lin, T. Y. Liu, M. C. Yang, *Biomaterials* **2004**, *25*, 1947.
[14] T. Y. Liu, W. C. Lin, L. Y. Huang, S. Y. Chen, M. C. Yang, *Biomaterials* **2005**, *25*, 1437.
[15] P. L. Ritger, N. A. Peppas, *J. Controlled Release* **1987**, *5*, 37.
[16] J. S. Ahn, H. K. Choi, M. K. Chun, J. M. Ryu, J. H. Jung, Y. U. Kim, C. S. Cho, *Biomaterials* **2002**, *23*, 1411.
[17] S. H. Hu, T. Y. Liu, D. M. Liu, S. Y. Chen, *Macromolecules* **2007**, *40*, 6786.
[18] S. H. Hu, T. Y. Liu, H. Y. Huang, D. M. Liu, S. Y. Chen, *Langmuir* **2008**, *24*, 239.